Fabrication of ZnPc/protein nanohorns for double photodynamic and hyperthermic cancer phototherapy

Minfang Zhang*[†‡], Tatsuya Murakami[§], Kumiko Ajima*, Kunihiro Tsuchida[§], Atula S. D. Sandanayaka[¶], Osamu Ito[¶], Sumio Iijima*[†‖], and Masako Yudasaka*[†‡‖]**

*Solution Oriented Research for Science and Technology, Japan Science and Technology, c/o NEC, 34 Miyukigaoka, Tsukuba, Ibaraki 305-8501, Japan; [†]Advanced Industrial Science and Technology, Central 5, 1-1-1 Higashi, Tsukuba, Ibaraki 305-8565, Japan; [§]Fujita Health University, 1-98 Dengakugakubo, Kutsukake-cho, Toyoake, Aichi 470-1192, Japan; [¶]Institute of Multidisciplinary Research for Advanced Materials, Tohoku University, Aoba-ku, Sendai 980-8577, Japan; [‖]NEC, 34 Miyukigaoka, Tsukuba, Ibaraki 305-8501, Japan; and **Meijo University, 1-501 Shiogamaguchi, Tenpaku-ku, Nagoya 468-8502, Japan

Edited by Mildred S. Dresselhaus, Massachusetts Institute of Technology, Cambridge, MA, and approved July 16, 2008 (received for review February 11, 2008)

Multifunctionalization of carbon nanotubules is easily achieved by attaching functional molecules that provide specific advantages for microscopic applications. We fabricated a double photodynamic therapy (PDT) and photohyperthermia (PHT) cancer phototherapy system that uses a single laser. Zinc phthalocyanine (ZnPc) was loaded onto single-wall carbon nanohorns with holes opened (SWNHox), and the protein bovine serum albumin (BSA) was attached to the carboxyl groups of SWNHox. In this system, ZnPc was the PDT agent, SWNHox was the PHT agent, and BSA enhanced biocompatibility. The double phototherapy effect was confirmed *in vitro* and *in vivo*. When ZnPc-SWNHox-BSA was injected into tumors that were subcutaneously transplanted into mice, the tumors almost disappeared upon 670-nm laser irradiation. In contrast, the tumors continued to grow when only ZnPc or SWNHox-BSA was injected. We conclude that carbon nanotubules may be a valuable new tool for use in cancer phototherapy.

carbon nanotubules | drug carrier | drug delivery system | nanoparticle | photohyperthermia

The biomedical applications of carbonaceous tubules, such as single-wall carbon nanotubes (SWNT) (1) and single-wall carbon nanohorns (SWNH) (2), are attracting attention. Pioneering *in vitro* studies have shown that SWNTs and SWNHs can be used to deliver therapeutic drugs and diagnostic molecules into cells (3–15). Carbonaceous tubules absorb light in the near-infrared region, and can cause cell death by a localized photothermal or photohyperthermia (PHT) effect (14). Using carbonaceous tubules, it would be straightforward to develop innovative multimodal therapies that combine PHT and chemotherapy or photodynamic therapies (PDTs). Because PDT is a noninvasive phototherapy (16–19) that is currently used clinically, combining PHT with PDT seems both feasible and likely to have clinical value. To determine whether PDT-PHT double phototherapy could be used as a cancer therapy, we loaded zinc phthalocyanine (ZnPc) as a PDT agent onto SWNHs with holes opened (SWNHox).

ZnPc is a promising photosensitizer for PDT (20–22) because of its high optical absorption coefficient in the 600- to 800-nm phototherapeutic window; this coefficient is higher than that of currently used porphyrin (16–19). However, ZnPc is hydrophobic and prone to self-aggregation in aqueous solutions, which drastically reduces the photosensitizing efficiency (23). To avoid the aggregation of ZnPc in aqueous solutions, an advanced delivery system is needed. To avoid the aggregation, we loaded ZnPc onto SWNHox, a novel drug carrier. SWNHox is graphitic tubule with a diameter of 2–5 nm and lengths of 40–50 nm (2) that have a relatively large inner space (24, 25) suitable for carrying drugs. Thousands of SWNHox partially coalesce to form an 80- to 100-nm spherical aggregate (2), and this aggregate is expected to have enhanced permeability and retention properties (26, 27) that make SWNHox effective for passive delivery of drugs to tumors. The holes of SWNHox observed with transmission electron microscopy (TEM) are 1–3 nm in diameter (28), and their pore sizes distributed in a range of 1–5 nm, showing a maximum at ≈2 nm (29), so that ZnPc [size: ≈1.4 nm (30)], similar to other molecules (7, 8, 31–33), can pass into the SWNHox tubules. The edges of the SWNHox holes have many carboxyl groups that can be used to attach biological materials, such as proteins, to enhance the biocompatibility of SWNHox (34).

Here, we prepared a ZnPc-SWNHox-BSA hybrid molecule by first loading SWNHox with ZnPc (ZnPc-SWNHox) and then attaching the protein bovine serum albumin (BSA) to the –COOH groups of SWNHox. The ZnPc and SWNHox functioned as the PDT and PHT agents, respectively, and BSA was used to improve the dispersion of the system in aqueous solution. We found that PDT-PHT double therapy using ZnPc-SWNHox-BSA had greater anticancer effects than either PDT using ZnPc or PHT using SWNHox-BSA. Remarkably, when the ZnPc-SWNHox-BSA was injected into tumors that were subcutaneously transplanted into mice and laser-irradiated, the tumors disappeared.

Currently, liposomes are used clinically as drug carriers, and polymer micelles and silica nanoparticles are potential carriers that have also been rigorously studied (35). These carriers have also been investigated as ZnPc carriers for PDT and have some advantages compared with ZnPc alone (36–39). However, these carriers do not absorb NIR-region light, and thus cannot themselves act as PHT agents. In contrast, gold nanoparticles (40) and gold nanoshells (41) do absorb NIR light and could be useful as PHT agents. However, the gold nanoparticles do not have nanospaces large enough to incorporate drugs and are difficult to modify. Thus, nanocarbon tubules are unique in their suitability for use as a PHT/PDT double therapy system, and we believe that the results presented here will stimulate advances in the use of nanocarbon tubules for drug delivery.

Results and Discussion

Characterization of ZnPc-SWNHox-BSA. ZnPc-SWNHox and ZnPc-SWNHox-BSA were fabricated according to the process depicted in Fig. 1*A*. SWNHox was prepared by light-assisted oxidation of SWNH using H_2O_2, which generates many carboxyl groups at the edges of the holes (34). ZnPc-SWNHox was

Author contributions: M.Z., S.I., and M.Y. designed research; M.Z., T.M., K.A., K.T., A.S.D.S., and O.I. performed research; M.Z., T.M., K.T., S.I., and M.Y. analyzed data; and M.Z. and M.Y. wrote the paper.

The authors declare no conflict of interest.

This article is a PNAS Direct Submission.

[‡]To whom correspondence may be addressed. E-mail: m-zhang@aist.go.jp or m-yudasaka@aist.go.jp.

This article contains supporting information online at www.pnas.org/cgi/content/full/0801349105/DCSupplemental.

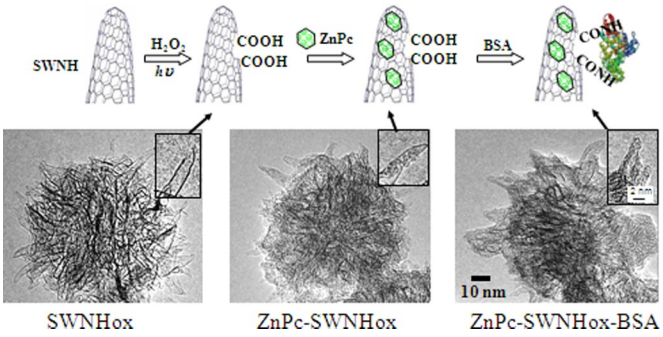

Fig. 1. Preparation of ZnPc-SWNHox-BSA. (*A*) Diagram showing steps in the production of ZnPc-SWNHox-BSA. The nanohorns were visualized by TEM at each stage of production. (*B*) SWNHox. (*C*) ZnPc-SWNHox. (*D*) ZnPc-SWNHox-BSA. (*Insets*) Magnified images.

prepared by immersing the SWNHox in a ZnPc solution. BSA was attached via diimide-activated amidation to the –COOH groups of SWNHox.

The structure of SWNHox observed in TEM images was similar to structures shown in previous reports: Both the spherical aggregates of SWNHox tubules (Fig. 1*B*) and the holes in the walls of SWNHox (Fig. 1*B Inset*) are visible. TEM revealed that ZnPc-SWNHox had a lot of ZnPc molecules located inside SWNHox, as well as some ZnPc molecules on the surface (Fig. 1*C*). The BSA molecules in ZnPc-SWNHox-BSA appeared to be located only on the outside surface of ZnPc-SWNHox (Fig. 1*D*).

To confirm the association of ZnPc and BSA with SWNHox, the elemental map on the ZnPc-SWNHox-BSA aggregate was measured with an energy-dispersive x-ray (EDX) spectrometer on a scanning transmission electron microscope (STEM). The STEM image of a ZnPc-SWNHox-BSA aggregate is shown in Fig. 2*A*, and the EDX elemental mapping images indicated that C, Zn, and O were present throughout the entire aggregate (Fig. 2 *B–D*). This confirmed that ZnPc and BSA were associated with SWNHox. The C was from SWNHox, BSA, and ZnPc, whereas the Zn was from ZnPc and the O was mainly from BSA.

Before testing the activities of ZnPc-SWNHox-BSA *in vitro* and *in vivo*, we checked absence of excess ZnPc that was not associated with SWNHox. First, we performed x-ray diffraction analysis and found no peaks originating from ZnPc crystals [supporting information (SI) Fig. S1], indicating that crystalline ZnPc was not present. This was also true for the ZnPc-SWNHox (Fig. S1). The absence of nonloaded ZnPc was further confirmed by comparing the quantities of ZnPc measured macroscopically by using thermogravimetric analysis (TGA) with the quantities measured microscopically in individual ZnPc-SWNHox-BSA aggregates, using an EDX spectrometer, which are described in detail in the following three paragraphs.

The each quantity of ZnPc, SWNHox, and BSA in ZnPc-SWNHox-BSA was estimated by TGA (Fig. 2*F*, red line). The ZnPc-SWNHox-BSA contained ≈26% BSA, as estimated from weight loss below 400°C, and ≈17% ZnPc as estimated from the TGA residue quantity at 1,000°C. In estimating the quantity of ZnPc, we used the TGA result of the intact ZnPc (Fig. 2*F*, blue line). Thus, ZnPc-SWNHox-BSA was composed of ZnPc (17%), SWNHox (57%), and BSA (26%) by weight.

We also measured the quantities of ZnPc and SWNHox in ZnPc-SWNHox (Fig. 2*F*, magenta line); ZnPc-SWNHox was composed of 24% ZnPc and 76% SWNHox by weight. Here, the quantity ratio of Zn to SWNHox in ZnPc-SWNHox was similar to that in ZnPc-SWNHox-BSA, which indicates that loaded ZnPc was not removed from ZnPc-SWNHox during the process of BSA attachment. The combustion temperature of the SWNHox in the complexes (ZnPc-SWNHox or ZnPc-SWNHox-BSA)

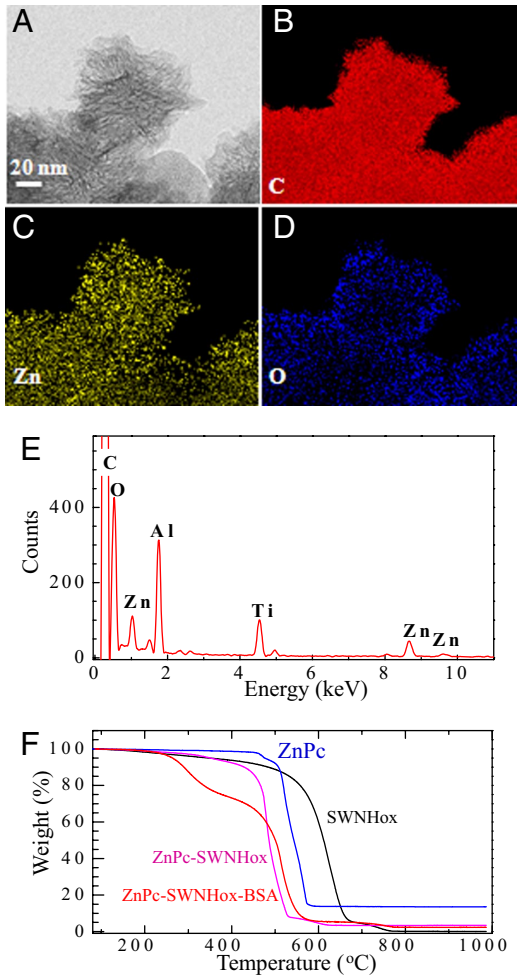

Fig. 2. Characterization of ZnPc-SWNHox-BSA by EDX and TGA. (*A*) Representative STEM image of one aggregate of ZnPc-SWNHox-BSA. (*B–D*) Atom-mapping images of C (*B*), Zn (*C*), and O (*D*). (*E*) Representative EDX spectra of ZnPc-SWNHox-BSA. (*F*) TGA results of SWNHox (black line), ZnPc powder (magenta line), SWNH-BSA (blue line), and ZnPc-SWNHox-BSA (red line).

was lower than that of SWNHox alone (Fig. 2*F*, black line), most likely because Zn catalyzed the combustion of SWNHox.

An EDX spectrum of one aggregate of ZnPc-SWNHox-BSA is shown in Fig. 2*E*. The peaks corresponding to Zn (1.01 and 8.63 keV), O (0.52 eV), and C (0.27 eV) are visible. The peak of N (0.38 eV) overlapped with the peak of C and could not be identified. Because the number of N atoms is much lower than the number of C atoms (C/N in ZnPc-SWNHox-BSA was ≈6.36/100, as calculated from their concentration and molecular structures), we used the peak C intensity without subtracting the N peak intensity to estimate the number ratio of Zn to C. We obtained a Zn/C number ratio of ≈0.45/100, where the C was from ZnPc, SWNHox, and BSA. The number ratio of Zn to C, as calculated from the TGA results described above, was 0.42/100. In these calculations, the molecular weight of BSA (66,000) and the number of C atoms (2932) in one BSA molecule were used (42). Because the number ratio of Zn to C obtained from EDX (0.45/100) was in close agreement with the number ratio derived from the TGA (0.42/100), we concluded that most of the ZnPc in the ZnPc-SWNHox-BSA was loaded onto SWNHox, supporting the absence of ZnPc that was not associated with the nanohorn aggregate.

BSA increased the dispersion of SWNHox-BSA in PBS (phosphate-buffered saline) versus SWNHox alone, as reported in ref.

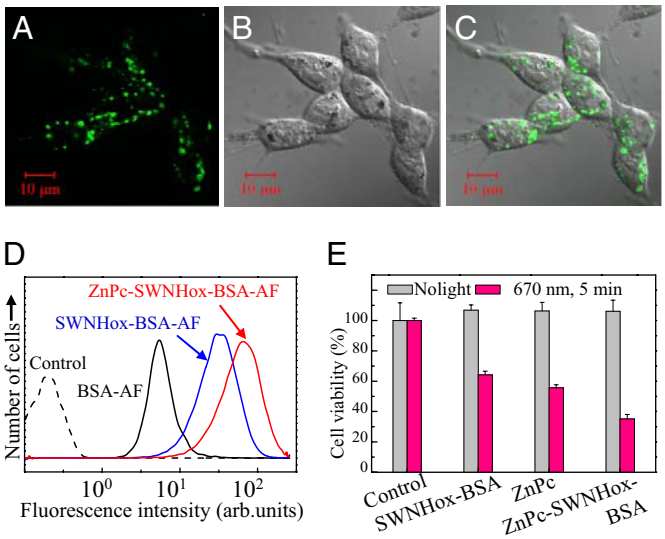

Fig. 3. Intracellular uptake and photodynamic and hyperthermic effects *in vitro*. The cellular uptake of ZnPc-SWNHox-BSA was investigated by confocal microscopy (excitation $\lambda = 488$ nm, emission detected at $\lambda = 510$ nm) after incubation of 5RP7 cells (transformed rat fibroblasts) with ZnPc-SWNHox-BSA-AF in the culture medium for 24 h. (*A*) Fluorescence image. (*B*) Differential interference contrast (DIC) image. (*C*) Combined fluorescence and DIC. (*D*) Flow cytometry of the 5RP7 cells. dashed black line, control; solid black line, incubated with BSA-AF; blue line, incubated with SWNHox-BSA-AF; red line, incubated with ZnPc-SWNHox-BSA-AF. (*E*) Photodynamic and hyperthermia destruction of 5RP7 cells. The viability of 5RP7 cells was estimated by using the WST-1 assay. The viabilities of the cells with and without laser irradiation (670 nm) for 5 min were indicated as red and blank bars, respectively.

34; we expected the same behavior for ZnPc-SWNHox-BSA. To test this, we prepared dispersed ZnPc-SWNHox-BSA in PBS by sonication for 3 min with a bath-type sonicator. Visual inspection indicated that this dispersion was stable for at least several weeks. The particle size of ZnPc-SWNHox-BSA, as estimated from dynamic light scattering measurements, was ≈160 nm (Fig. S2). ZnPc-SWNHox-BSA was larger than the particle size of SWNHox-BSA, which is ≈110 nm (34). Thus, the ZnPc-SWNHox-BSA was not quite as dispersed as SWNHox-BSA. This is because a drying process to remove DMSO and ethanol is applied to ZnPc-SWNHox before its modification with BSA; this process could induce ZnPc-SWNHox/ZnPc-SWNHox adhesion. In contrast, SWNHox was not subjected to this process because it was not modified with BSA.

Intracellular Uptake and Photodynamic and Hyperthermia Effects *in Vitro*. We previously reported that conjugation to BSA enhanced the uptake of SWNHox by H460 cells (non-small-cell human lung cancer cells) (34); therefore we expected that ZnPc-SWNHox-BSA would also be readily taken up by 5RP7 cells (rat fibroblasts transformed by the c-Ha-ras oncogene). For *in vitro* testing, we attached BSA labeled with Alexa Fluor 488 dye (BSA-AF) to SWNHox and ZnPc-SWNHox to generate SWNHox-BSA-AF and ZnPc-SWNHox-BSA-AF. 5RP7 cells were incubated in medium containing SWNHox-BSA-AF or ZnPc-SWNHox-BSA-AF (ZnPc, 5 μM) for 24 h, and then the cells were observed by using confocal microscopy. The images taken at the middle plane of the cells showed a green signal from SWNHox-BSA-AF (not shown) or ZnPc-SWNHox-BSA-AF (Fig. 3 *A–C*) inside of the cells. The flow cytometry measurements (Fig. 3*D*) revealed that almost 100% of the cells took up SWNHox-BSA-AF or ZnPc-SWNHox-BSA-AF, a much larger percentage than for the control, BSA-AF, which was in 36% of the cells.

After incubation of the 5RP7 cells for 24 h in culture medium containing ZnPc-SWNHox-BSA (0.02 mg/ml; ZnPc, 5 μM), we used the 670-nm laser to irradiate the cells for 5 min at ≈37°C. Irradiation greatly decreased cell viability to ≈34%, as determined by the WST-1 assay (Fig. 3*E*). Without irradiation, viability did not decrease (Fig. 3*E*). The lethal effect of light irradiation was weaker when ZnPc or SWNHox-BSA rather than ZnPc-SWNHox-BSA was used: Cell viability decreased to ≈59% or 68% for ZnPc or SWNHox-BSA, respectively (Fig. 3*E*). Thus, double PDT-PHT therapy with ZnPc-SWNHox-BSA killed more 5RP7 cells *in vitro* than did PDT therapy alone (with ZnPc) or PHT therapy alone (using SWNHox-BSA).

Photodynamic and Hyperthermia Double Therapy Using ZnPc-SWNHox-BSA *in Vivo*. For *in vivo* studies, 5RP7 cells were subcutaneously transplanted into both the left and right flanks of nude mice. Seven days after transplantation (i.e., on day 7), each tumor was injected a single time with 200 μl of PBS or 200 μl of a PBS dispersion of ZnPc (50 μM), SWNHox-BSA (0.15 mg/ml), or ZnPc-SWNHox-BSA (0.17 mg/ml, 50 μM). After injection, the tumors on the left flanks were irradiated for 15 min every 24 h for 10 days by using a 670-nm laser (Fig. 4*A*). The transplanted tumors on the right flanks were not irradiated.

Without laser irradiation, the tumor volumes increased over time, regardless of the substance injected into the tumors (Fig. 4*B*, right flank, and *D*). However, laser irradiation after injection of ZnPc-SWNHox-BSA markedly suppressed tumor growth (Fig. 4*C*, red line). Irradiation after injection of SWNHox-BSA (Fig. 4*C*, blue line) and ZnPc (Fig. 4*C*, magenta line) also suppressed tumor growth more than injection of PBS (Fig. 4 *C* and *D*, black lines), but less than after injection of ZnPc-SWNHox-BSA. When ZnPc-SWNHox-BSA was injected before irradiation, the tumor size decreased on day 15 and disappeared by day 17 (Fig. 4*C*, red line, and Fig. 4*B*, left flank). Furthermore, the tumor did not reappear after laser irradiation was stopped on days 19–21 (Fig. 4*C*, red line). When ZnPc or SWNHox-BSA was injected, tumor growth was suppressed, but the tumors did not disappear (Fig. 4*C*, magenta and blue lines). These results indicate that PDT using ZnPc or PHT using SWNHox-BSA both inhibited tumor growth, but PDT-PHT double phototherapy using ZnPc-SWNHox-BSA killed tumor cells much more effectively, resulting in the macroscopic disappearance of the tumor. It should be noted that despite the anticancer effect of ZnPc-SWNHox-PBS, the body weights of the mice increased continuously during the test period, indicating that there were no side effects that caused weight loss (Fig. S3).

The dark spots that appeared on the left flank of irradiated mice (Fig. 4*B*) were due to the hemorrhage caused by laser irradiation. Because the sizes of the PBS-injected tumors that were irradiated by the laser (Fig. 4*C*, black line) were similar to those of the PBS-injected tumors that were not irradiated (Fig. 4*D*, black line), it appears that laser irradiation alone inhibited tumor growth very weakly under the conditions used here.

Mechanisms of Photophysics and Photothermal Effects. It is generally accepted that optically excited photosensitizers transfer energy to oxygen molecules to generate singlet oxygen species that destroy tumor cells (17–19). However, we found that the 670-nm laser irradiation of ZnPc-SWNHox-BSA did not generate singlet oxygen in our study. The generation of singlet oxygen was examined by a chemical method using anthracene-9,10-dipropionic acid disodium salt (ADPA). ADPA is a fluorescent material that selectively reacts with singlet oxygen and changes to a non-fluorescent peroxide (43). In the presence of singlet oxygen, the ADPA fluorescence is quenched and its absorption, for example at 358, 378, and 400 nm, is diminished. However, when ADPA was mixed with the solution of dispersed ZnPc-SWNHox-BSA in PBS and irradiated with 650–750 nm light by

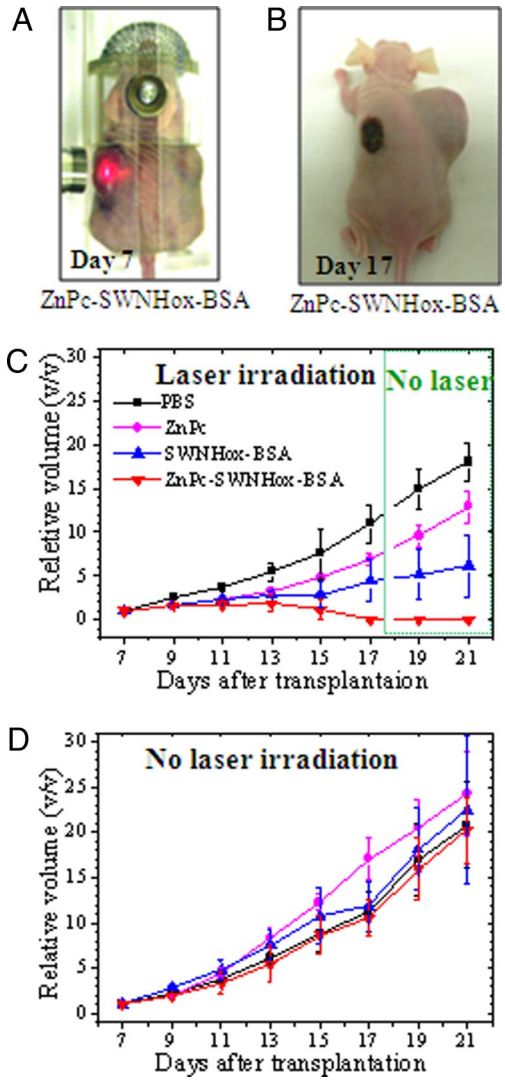

Fig. 4. Photodynamic and hyperthermic destruction of tumors *in vivo*. (*A*) A mouse with large tumors on its left and right flanks 7 days after tumor cell transplantation (day 7). The tumor on the left flank is being irradiated with 670-nm laser. (*B*) A mouse after 10 days of treatment (day 17) with ZnPc-SWNHox-BSA and laser irradiation of the tumor on its left flank. (*C*) Relative volumes of tumors on the left flanks. PBS (black line) or PBS dispersions of ZnPc (magenta line), SWNHox-BSA (blue line), or ZnPx-SWNHox-BSA (red line) were intratumorally injected and treated with 670-nm laser. (*D*) Relative volumes of tumors on the right flanks that were injected by PBS (black line) or PBS dispersions of ZnPc (magenta line), SWNHox-BSA (blue line), or ZnPx-SWNHox-BSA (red line) but not subjected to laser irradiation.

using a Xe lamp with a band pass filter for ≈10 min, the ADPA absorption spectra did not change (Fig. S4*a*). This means that singlet oxygen was not generated by the laser irradiation of the dispersion of ZnPc-SWNHox-BSA in PBS.

Optical absorption spectra of the aqueous solution of ZnPc-SWNHox-BSA showed absorption bands at 602 and 666 nm, which are characteristic of ZnPc. These absorption bands red-shifted to 635 and 710 nm, respectively, and the bandwidth broadened compared with those of ZnPc dissolved in ethanol (Fig. S4*b*). These data indicate that ZnPc interacted strongly with SWNHox.

We performed experiments to investigate the energy/electron transfer processes involving ZnPc-SWNHox-BSA in greater detail [see *SI Text* (*Photoinduced charge-transfer in the ZnPc-SWNHox-BSA system and potential reactive oxygen generation*) and Figs. S5 and S6]. We found that when ZnPc was excited by light, electrons were transferred to SWNHox and formed a charge separation state in the ZnPc-SWNHox-BSA system. When methyl viologen dication (MV^{2+}) and an appropriate hole-shifter were added to the ZnPc-SWNHox-BSA dispersion, reduced methyl viologen (MV^{+}) was generated upon laser irradiation (Fig. S4*c*). The results were consistent with studies of electron transfer from optically excited ZnP molecules to fullerenes (44, 45), carbon nanotubes (46, 47), and SWNHs (48). When oxygen is present, it can accept electrons from the charge separated state of ZnPc-SWNHox-BSA to generate $O_2^{\bullet -}$ and, subsequently, other reactive species such as hydroxyl radicals (49–51). The presence of these reactive species leads to the death of nearby cancer cells.

To confirm the photothermal effect, we monitored the temperature of PBS solutions of dispersed ZnPc-SWNHox-BSA and SWNHox-BSA during 670-nm laser irradiation (Fig. S7). The concentrations of SWNHox-BSA in the PBS dispersion of ZnPc-SWNHox-BSA and SWNHox-BSA were 0.08, 0.008, and 0.0008 mg/ml. These concentrations were similar to those used in the cell assays and in the mouse tests, and the dispersions were placed in a 37°C incubator to mimic the cell assay and animal testing conditions. The temperature of the dispersions increased with the duration of laser irradiation and increased to >41°C in ≈2–4 min, depending on the specimen concentration (Fig. S7). It is known that in the hyperthermic treatment of tumors, heating to 40–43°C can destroy the tumor cells (52, 53). Therefore, it appears that both ZnPc-SWNHox-BSA and SWNHox-BSA have photothermal conversion efficiencies high enough to act as PHT agents. The similar increases in temperature upon irradiation of solutions of ZnPc-SWNHox-BSA and SWNHox-BSA (Fig. S7) indicate that the ZnPc did not contribute to the PHT effect, and that the observed PHT effect was mainly due to SWNHox. In addition, we note that the temperature increased by PHT at the tumor sites was not decreased by blood circulation because of its poor circulation; however, at other sites, blood circulation effectively cools the tissue, allowing selective tumor death by PHT (52, 53). Results of a tissue-mimicking phantom experiment with 0.001% (by weight) SWNHox indicated that even with normal blood flow, the temperature of the tissue might still increase up to 6°C upon laser irradiation [see *SI Text* (*Agar Tissue-Mimicking Phantom Experiment*) and Figs. S8 and S9].

Conclusions

We developed a ZnPc-SWNHox-BSA double phototherapy system using the unique characteristics of SWNHox and showed that PDT-PHT using a single laser (670 nm) was both feasible and effective. In this PDT-PHT system, ZnPc acted as the PDT agent, SWNHox-BSA acted as the PHT agent, in which BSA made the system hydrophilic and biocompatible. When ZnPc-SWNHox-BSA was injected into tumors that were subcutaneously transplanted into mice, subsequent laser irradiation for 15 min every 24 h for 10 days caused the tumors to disappear. Although PDT treatment alone using ZnPc or PHT treatment alone using SWNHox-BSA had some antitumor effects, the effects were less than that with double PDT-PHT treatment, both in the cell assay and *in vivo*; using PDT or PHT alone, the tumors in the mice never disappeared.

It is important to emphasize that the PDT-PHT double therapy system was only possible with carbon nanotubules. The carbon nanotubules have PHT effects by themselves and additionally provide a platform for attachment/loading of PDT agents. Such agents can be either stored/adsorbed onto the nanotubules, or chemically bonded. The carbon nanotubules have the potential to be made more multifunctional: Here, we attached BSA to the SWNHox to enhance biocompatibility, but it would also be possible to attach tumor targeting moieties for i.v. delivery to tumors.

Methods

Sample Preparation and Structural Analysis. ***SWNHox.*** The SWNHs were produced by laser vaporization of pure graphite in an Ar atmosphere at room temperature without using any metal catalysts (2). The content of SWNHs was ≈95% with remaining graphitic particles (5%) (54). We treated as-grown SWNHs with light-assisted oxidation to open holes and introduced abundant carboxyl groups at the edges of the holes (34). Briefly, a dispersed solution of ≈40 mg of as-grown SWNHs in 50 ml of 30% H_2O_2 aqueous solution was stirred at 250 rpm on a hot plate set at 100°C and irradiated with a 150-W Xe lamp (wavelength, 250–2,000 nm) for 2.5 h. The resulting SWNHox was filtered, washed with sterilized deionized water three to five times, and freeze-dried. ***ZnPc-SWNHox.*** A ZnPc-saturated solution was prepared by dissolving 10 mg of ZnPc (CAS 1432-04-8; Sigma–Aldrich) in a 100-ml mixture of dimethyl sulfoxide and ethanol (1:1 by volume). After leaving for 24 h, the supernatant was decanted (≈90 ml was recovered). SWNHox (10 mg) was dispersed by sonication in the ZnPc-saturated solution of dimethyl sulfoxide and ethanol (90 ml). After stirring for 48 h, the solution was filtered and solid powder was obtained. The powder was redispersed in ethanol by sonication for 2–3 min and filtered again to remove excess ZnPc. The resulting ZnPc-SWNHox was freeze-dried. ***ZnPc-SWNHox-BSA and SWNHox-BSA.*** ZnPc-SWNHox was chemically modified with BSA ($C_{2932}H_{4614}N_{780}O_{898}S_{39}$, 66 kDa; Sigma–Aldrich) via diimide-activated amidation (34, 55). We dispersed 40 mg of freeze-dried ZnPc-SWNHox in 50 ml of PBS (Sigma, D8537) with a bath-type sonicator for 30 min, then added 100 mg of 1-ethyl-3-(3-dimethylaminopropyl)carbodiimide (EDAC) (Sigma–Aldrich) followed by stirring for 2 h. BSA (200 mg) was added to the dispersion of SWNHox and stirred at room temperature for 24 h. Nonreacted EDAC and BSA were removed by repeated filtration and dispersion in sterilized water. Without drying, the powder on the filter paper was dissolved in PBS for subsequent *in vitro* and *in vivo* experiments. The quantity of ZnPc-SWNHox-BSA in the PBS was determined by the emission intensity of Zn measured with inductively coupled plasma optical emission spectroscopy (HORIBA ULTIMA2). For TGA, XRD, and electron spectroscopic observations, the samples were freeze-dried after filtration.

The SWNHox-BSA (without ZnPc-loading) was prepared by attaching BSA to SWNHox, using the process described above.

For the cellular uptake experiments, we used ZnPc-SWNHox-BSA-AF and SWNHox-BSA-AF. BSA-AF refers to Alexa Fluor 488-labeled BSA (Molecular Probes).

Structures and Components. The structure and chemical components of the prepared specimens were investigated after drying at 70°C for 48 h in air. TGA (TGA 2950; TA Instruments) was carried out in oxygen gas (100%) at a temperature elevation rate of 10°C/min. TEM (002B; Topcon) was observed at an acceleration voltage of 120 kV with a 36-μA current. A STEM equipped with EDX (HD 2300; Hitachi) was operated at 120 kV and 74 μA, and the elemental map was obtained by using a scanning spot size of 0.5 nm and a scanning rate of 0.5 nm/ms. The EDX spectrum for each aggregate was measured, and the number ratio of Zn/C was averaged from 10 such measurements.

Optical Spectra of ZnPc-SWNHox-BSA. ZnPc-SWNHox-BSA was dispersed in PBS (ZnPc, 0.1 mg/ml), and ZnPc was dispersed in ethanol (0.1 mg/ml). The optical absorption spectra were measured by using a UV-Vis-NIR spectrometer (Lambda 19; PerkinElmer).

We also determined whether singlet oxygen was generated in the PBS dispersion of ZnPc-SWNHox-BSA or not when irradiated with 650–750 nm light. The PBS dispersion of ZnPc-SWNHox-BSA (ZnPc, ≈10 μM) was mixed with the PBS solution of anthracene-9,10-dipropionic acid disodium salt (Molecular Probes) (10 μM; volume ratio of 1:1). The absorption spectra were measured with a UV-Vis-NIR before and after 650- to 750-nm light irradiation (Xe lamp; bandpass filters of 650–750 nm).

Photothermal Effects. ZnPc-SWNHox-BSA or SWNHox-BSA/PBS dispersions (3 ml; 0.1–0.001 mg/ml) in quartz cells ($1 \times 1 \times 4$ cm^3) were placed in an incubator (air, 37°C). A laser with a wavelength of 670 nm (power, 160 mW; spot diameter, 5 mm) from a fiber-coupled laser system (BWF-670-300E; B&W Tek) was used to irradiate the top surface of the dispersion for 0–20 min. The temperature was measured by a chromel-alumel thermocouple thermometer (probe diameter, 0.25 mm).

Phototherapy *in Vitro*. This study used 5RP7 cells, which are rat fibroblasts transformed by the c-Ha-ras oncogene (Health Science Research Resources Bank, Inc.). Cells were cultured in monolayer at 37°C in a humidified atmosphere with 5% CO_2. The cell culture medium was DMEM (Sigma) supplemented with 10% fetal BSA (American Type Culture Collection) and 0.1% penicillin-streptomycin (GIBCO).

To investigate the uptake of ZnPc-SWNHox-BSA by 5RP7 cells, we seeded the cells in 35-mm glass dishes at a density of 2×10^4 cells per cm^2 in the culture medium (3 ml) and incubated the dishes for ≈24 h. The culture medium was removed and replaced with culture medium containing ZnPc-SWNHox-BSA-AF (ZnPc, 5 μM), and incubated for a further 24 h. After incubation, the culture medium was removed and cells were rinsed twice with PBS; fresh culture medium lacking ZnPc-SWNH-BSA-AF was added. The cells were observed by confocal microscopy (LSM 5 PASCAL; Zeiss) or, alternatively, detached from the dishes by using 0.25% trypsin-EDTA (Sigma–Aldrich) and redispersed in culture medium for flow cytometry (Beckman Cytomics FC500) analysis. The excitation wavelength was 488 nm, and the fluorescence emission was detected at 525 nm.

Phototherapy efficiency was examined as follows. We cultured 5RP7 cells in 96-well plates (2×10^4 cells per ml, 100 μl per well) for 24 h. The culture medium was replaced by medium containing ZnPc-SWNHox-BSA (ZnPc, 5 μM; SWNHox, 0.017 mg/ml), ZnPc (ZnPc, 5 μM), and SWNHox-BSA (0.02 mg/ml). After the cells incubated for 24 h, we used a fiber-coupled laser system (the same one used for determining photothermal effects) to irradiate the cells for 5 min at 37°C inside the incubator. After irradiation, we added 10 μl of WST-1 agent (Sigma–Aldrich) and incubated the cells for ≈1 h. The cell viability was estimated by using a Microplate Reader 680 (Bio-Rad).

Phototherapy *in Vivo*. Nude 6-week-old mice ($n = 16$; BALB/cAJc1-nu/nu mice) were purchased from CLEA Japan. The mice were bilaterally implanted with 5RP7 cells (1×10^6) via subcutaneous injection into each flank when they were 8 weeks old. Seven days after implantation, the mice were separated into four groups (four mice per group), and the tumors were injected with 200 μl of PBS or 200 μl of the PBS dispersions of ZnPc-SWNHox-BSA, ZnPc, or SWNHox-BSA. The concentration of ZnPc was set to be ≈50 μM. The SWNHox concentration in the SWNHox-BSA/PBS suspension and ZnPc-SWNHox-BSA/PBS suspension was ≈0.15 mg/ml. From day 7, the tumors on the left flanks only were irradiated every 24 h with the 670-nm laser. The laser was the same one used in the photothermal study and for the *in vitro* PDT test. Because the tumors were much larger than the spot size of the laser (≈5 mm), we irradiated each tumor in five locations (3 min per location) for a total of 15 min of irradiation. The only exception was the first day, when we irradiated only one spot per tumor for 15 min. We recorded body weight and tumor size for each mouse during the treatment; i.e., for the 10 days of treatment and for two additional days once treatment was over. The size of the tumor was measured at the widest point (W) and along the corresponding perpendicular length (L). The formula for computing tumor volume (V) was for a standard volume of an ellipsoid, where $V = 4\pi/3$ (length/2 × width/2 × depth/2). Assuming that depth equals width and π equals 3, $V = 1/2 \times L \times W^2$. The relative tumor volume was calculated as (tumor volume on the day of measurement)/(volume of the tumor on the day 7). On day 7, the tumor volumes ranged from 200 to 600 mm^3. When the tumors disappeared, the tumor volumes were recorded as ''zero.''

ACKNOWLEDGMENTS. We thank Dr. Azaimi, Dr. Kasuya for providing single-wall carbon nanohorns, and Dr. Miyawaki and Dr. Maigne for assistance with measurements with inductively coupled plasma optical emission spectroscopy and scanning transmission electron microscope.

1. Iijima S, Ichihashi T (1993) Single-shell carbon nanotubes of 1-nm diameter. *Nature* 363:603–605.
2. Iijima S, *et al.* (1999) Nano-aggregates of single-walled graphitic carbon nano-horns. *Chem Phys Lett* 309:165–170.
3. Kam NWS, Jessop T, Wender P, Dai H (2004) Nanotube molecular transporters: Internalization of carbon nanotube-protein conjugates into mammalian cells. *J Am Chem Soc* 126:6850–6851.
4. Lu Q, *et al.* (2004) RNA polymer translocation with single-walled carbon nanotubes. *Nano Lett* 4:2473–2477.
5. Pantarotto D, Briand J, Prato M, Bianco A (2004) Translocation of bioactive peptides across cell membranes by carbon nanotubes. *Chem Commun* 1:16–17.
6. Teker K, Sirdeshmukh R, Panchapakesan B (2004) Antibody functionalization of carbon nanotubes for breast cancer applications. *Sensors Proc IEEE* 2:(24–27):814–817.
7. Murakami T, *et al.* (2004) Drug-loaded carbon nanohorns: Adsorption and release of dexamethasone in vitro. *Mol Pharmacol* 1:399–405.
8. Ajima K, *et al.* (2005) Carbon nanohorns as anticancer drug carriers. *Mol Pharmacol* 2:475–480.
9. Kam NWS, Dai H (2005) Carbon nanotubes as intracellular protein transporters: Generality and biological functionality. *J Am Chem Soc* 127:6021–6026.
10. Singh R, *et al.* (2005) Binding and condensation of plasmid DNA onto functionalized carbon nanotubes: Toward the construction of nanotube-based gene delivery vectors. *J Am Chem Soc* 127:4388–4396.

11. Bianco A, Kostarelos K, Prato M (2005) Application of carbon nanotubes in drug delivery. *Curr Opin Chem Biol* 9:674–679.
12. Bianco A, Kostarelos K, Partidos CD, Prato M (2005) Biomedical application of functionalised carbon nanotubes. *Chem Commun* 5:571–577.
13. Wu W, *et al.* (2005) Targeted delivery of amphotericin B to cells by using functionalized carbon nanotubes. *Angew Chem Int Ed* 44:6358–6362.
14. Kam NWS, O'Connell M, Wisdom JA, Dai H (2005) Carbon nanotubes as multifunctional biological transporters and near-infrared agents for selective cancer cell destruction. *Proc Natl Acad Sci USA* 102:11600–11605.
15. Klumpp C, Kostarelos K, Prato M, Bianco A (2006) Functionalized carbon nanotubes as emerging nanovectors for the delivery of therapeutics. *Biochim Biophys Acta Biomembr* 1758:404–412.
16. Dougherty TJ, Kaufman JE, Goldfarb A (1978) Photoradiation therapy for the treatment of malignant tumors. *Cancer Res* 38:2628–2636.
17. Dougherty TJ, *et al.* (1992) *Photodynamic Therapy* (Dekker, New York), pp 1–15.
18. Dougherty TJ, *et al.* (1998) Photodynamic therapy. *J Natl Cancer Inst* 90:889–905.
19. Moan J (1986) Porphyrin photosensitization and phototherapy. *Photochem Photobiol* 43:681–690.
20. Owens JW, Smith R, Robinson R, Robins M (1998) Photophysical properties of porphyrins, phthalocyanines and benzochlorins. *Inorg Chem Acta* 279:226–231.
21. Cahn W, Brasseur N, La Madeleine C, Quellet R, Van Lier JE (2001) Current states of phthalocyanines in the photodynamic therapy of cancer. *Eur J Cancer* 33:1855–1860.
22. Dougherty TJ (1996) A brief history of clinical photodynamic therapy development at Roswell Park Cancer Institute. *J Clin Laser Med* 14:219–221.
23. Dhami S, Philips D (1996) Comparison of the photophysics of an aggregation and none aggregation aluminum phthalocyanine system incorporated into unilamellar vesicles. *J Photochem Photobiol A* 100:77–84.
24. Murata K, *et al.* (2001) Molecular potential structures of heat-treated single-wall carbon nanohorn assemblies. *J Phys Chem B* 105:10210–10216.
25. Yang C, *et al.* (2005) Highly ultramicrosporous single-walled carbon nanohorn assemblies. *Adv Mater* 17:866–870.
26. Maeda H (1992) The tumor blood vessel as an ideal target for macromolecular anticancer agents. *J Controlled Release* 19:315–324.
27. Maeda H (2001) The enhanced permeability and retention (EPR) effect in tumor vasculature: The key role of tumor-selective macromolecular drug targeting. *Adv Enzyme Regul* 41:189–207.
28. Ajima K, *et al.* (2004) Material storage mechanism in porous nanocarbon. *Adv Mater* 16:397–401.
29. Miyawaki J, Yuge R, Kawai T, Yudasaka M, Iijima S (2007) Evidence of thermal closing of atomic-vacancy holes in single-wall carbon nanohorns. *J Phys Chem C* 111:1553–1555.
30. Kawabe E, *et al.* (2004) The study of epitaxial growth of phthalocyanine-related molecular films deposited on GeS(001). *IPAP Conf Ser* 6:95–98.
31. Hashimoto A, *et al.* (2004) Selective deposition of a gadolinium (III) cluster in a hole opening of single-wall carbon nanohorn. *Proc Natl Acad Sci USA* 101:8527–8530.
32. Yuge R, *et al.* (2004) Preferential deposition of Pt nanoparticles inside single-walled carbon nanohorns. *Adv Mater* 16:1420–1423.
33. Murata K, *et al.* (2002) Nanowindow-induced molecular sieving effect in a single-wall carbon nanohorn. *J Phys Chem B* 106:12668–12669.
34. Zhang M, Yudasaka M, Ajima K, Miyawaki J, Iijima S (2007) Light-assisted oxidation of single-wall carbon nanohorns for abundant creation of oxygenated groups that enable chemical modifications with proteins to enhance biocompatibility. *ACS Nano* 1:265–272.
35. Ranade V, Hollinger (2004) *Drug Delivery System* (CRC, Boca Raton, FL), 2nd Ed.
36. Derycke AS, DE Witte PA (2004) Liposomes for photodynamic therapy. *Adv Drug Deliv Rev* 56:17–30.
37. Chen B, Pogue B, Hasan T (2005) Liposomal delivery of photosensitizing agents. *Exp Opin Drug Deliv* 2:477–487.
38. McCarthy J, Perez J, Bruckner C, Weissleder R (2005) Polymeric nanoparticle preparation that eradicates tumors. *Nano Lett* 5:2552–2556.
39. Roy I, *et al.* (2003) Ceramic-based nanoparticles entrapping water-insoluble photosensitizing anticancer drugs: A novel drug-carrier system for photodynamic therapy. *J Am Chem Soc* 125:7860–7865.
40. Everts M, *et al.* (2006) Covalently linked Au nanoparticles to a viral vector: Potential for combined photothermal and gene cancer therapy. *Nano Lett* 6:587–591.
41. O'Neal D, Hirsch L, Halas N, Payne J, West J (2004) Photo-thermal tumor ablation in mice using near infrared-absorbing nanoparticles. *Cancer Lett* 209:171–176.
42. Peters T, Jr (1985) Serum albumin. *Adv Protein Chem* 37:161–245.
43. Lindig BA, Rogers M-J, Schaap AP (1980) Determination of the lifetime of singlet oxygen in D_2O using 9,10-anthracene dipropionic acid. *J Am Chem Soc* 102:5590–5593.
44. El-Khouly ME, Araki Y, Fujitsuka M, Watanabe A, Ito O (2001) Photoinduced electron transfer between chlorophylls (alb) and fullerenes (C_{60}/C_{70}) studied by laser flash photolysis. *J Photochem Photobiol* 74:22–30.
45. D'Souza F, Ito O (2005) Photoinduced electron transfer in supramolecular systems of fullerenes functionalized with ligands capable of binding to zinc porphyrins and zinc phthalocyanines. *Coord Chem Rev* 249:1410–1422.
46. Guldi DM, Taieb H, Aminur Rahman GM, Tagmatarchis N, Prato M (2005) Novel photoactive single-walled carbon nanotube-porphyrin polymer wraps: Efficient and long-lived intracomplex charge separation. *Adv Mater* 17:871–875.
47. Baskaran D, Mays JW, Zhang X, Bratcher MS (2005) Carbon nanotubes with covalently linked porphyrin antennae: Photoinduced electron transfer. *J Am Chem Soc* 127:6916–6917.
48. Sandanayaka A-D, *et al.* (2007) Photoinduced electron-transfer processes of carbon nanohorns with covalently linked pyrene chromophores: Charge-separation and electron-migration systems. *J Mater Chem* 17:2540–2546.
49. Mates JM, Sanchez-Jimenez FM (2000) Role of reactive oxygen species in apoptosis: Implications for cancer therapy. *Int J Biochem Cell Biol* 32:157–170.
50. Bandyopadhyay U, Das D, Banerjee R (1999) Reactive oxygen species: Oxidative damage and pathogenesis. *Curr Sci* 77:658–666.
51. Wiseman H, Halliwell B (1996) Damage to DNA by reactive oxygen and nitrogen species: Role in inflammatory disease and progression to cancer. *Biochem J* 313:17–29.
52. Alpard SK, *et al.* (1996) Therapeutic hyperthermia. *Perfusion* 11:425–435.
53. Wust P, *et al.* (2002) Hyperthermia in combined treatment of cancer. *Lancet Oncol* 3:487–497.
54. Azami T, *et al.* (2008) Large-scale production of single-wall carbon nanohorns with high purity. *J Phys Chem C* 112:1330–1334.
55. Huang W, *et al.* (2002) Attaching proteins to carbon nanotubes via diimide-activated amidation. *Nano Lett* 2:311–314.